Fundamental limitations of THz and Niobiumnitride SIS mixers

Dieleman, Pieter

Chapter 4

DC heating in SIS junctions

DC heating effects in Superconductor- Insulator- Superconductor (SIS) tunnel junctions are studied by comparing junctions sandwiched between niobium or aluminum layers. With niobium a temperature rise of several Kelvin is observed, which is reduced by an order of magnitude by using aluminum. A simple model satisfactorily explains this observation and predicts a 30% increase in the subgap current due to the elevated temperature. At the operating voltage for heterodyne mixing the mixer noise temperature increases by only 2%.

4.1 Introduction

In recent years superconductor-insulator-superconductor (SIS) tunnel junctions are increasingly being used up to terahertz frequencies. At present the highest frequency has been 1100 GHz[1,2] which is well beyond the gap frequency of niobium indicating that the principle of operation (photon-assisted tunneling) is not intrinsically limited by the energy gap of niobium (700 GHz). However in operating at these high frequencies it has recently been observed[3,4] that the photon-assisted tunneling step above the gap occurs at a smaller value than expected, indicating a depressed gap due to intrinsic heating by the bias-current. (See Fig 4.2, insert). From a practical point of view this effect could result in an increased subgap current and correspondingly extra noise when irradiated. For this reason we have studied photon-assisted tunneling and heterodyne mixing up to terahertz frequencies using both all-niobium tunnel junctions and niobium tun-

nel junctions with aluminum wiring layers.

4.2 Junction layout

The SIS junctions considered here consist of 100 nm thick Nb layers with an Al_2O_3 tunnel barrier in between. Fabrication details are described elsewhere[5]. The junctions are sandwiched between leads consisting of either 200 nm thick Nb (lower layer) and 600 nm Nb (upper layer) or of 85 nm Al with 20 nm Nb (lower layers) and 85 nm Al with 400 nm Nb in parallel (upper layers)[1] as schematically shown in Fig. 4.1.

In this paper we will first analyze theoretically the heat flow and compare it with experimental results.

4.3 Heat flow

We assume that the heat transport in the leads can be described by the following differential equation[6]:

$$-K(r^2\frac{d^2T}{dr^2} + r\frac{dT}{dr}) + \frac{Y}{d}r^2(T - T_{bath}) = 0 \qquad (4.1)$$

in which T is an equilibrium electron temperature. The heat input I·V is radially transported away from the junction region in two ways: by thermal conduction K in the metal films (the first term) and by heat transfer Y towards the substrate (the second term). The thickness of the leads is denoted by d, T_{bath} is the temperature of the substrate. The heating is taken to be due to the DC current only since it was experimentally observed that varying the RF power had no influence on the junction temperature[7]. We also assume that T is constant in a cylinder of radius $r = w/2$, where w is the width of the junction (See Fig. 4.1). Boundary conditions are:

$$\begin{aligned} -K\ \tfrac{dT}{dr} &= \tfrac{I\cdot V}{\pi\ w\ d\ (\cdot 2)} && (r = \tfrac{w}{2}) \\ T &= T_{bath} && (r \Rightarrow \infty) \end{aligned}$$

The factor 2 in the denominator of the first equation accounts for the fact that the heat flow is radial in a half plane only in the top lead. (See Fig. 4.1(a)).

The thermal conductivity K of the metal films is estimated from the measured electrical resistivities (above Tc) by the Wiedemann-Franz law. The thermal con-

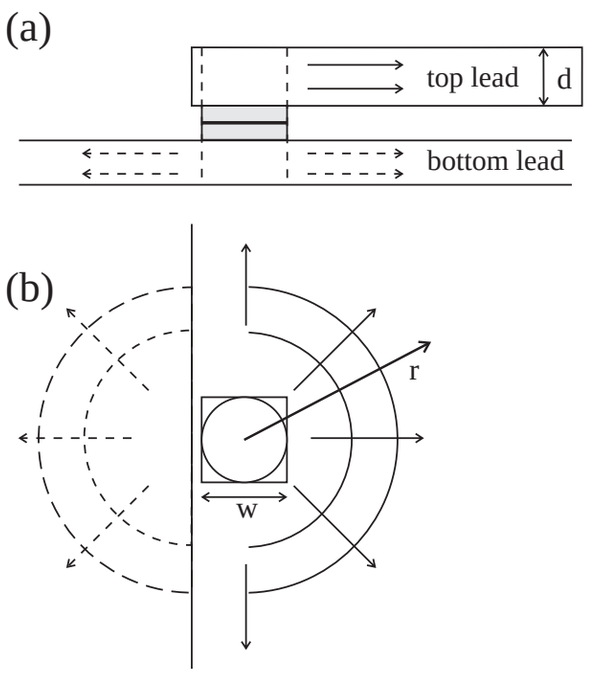

FIGURE 4.1. Schematic layout of the junction sandwiched between the leads. **(a)**: side view, **(b)**: top view. The arrows indicate the radial heat flow.

ductivity of Nb[8] is corrected for the decrease in the quasiparticle density by a prefactor $T/1.55 \cdot \exp(-1.76\mathrm{Tc}/T)$[9]. (See Table 4.1).

4.4 Heat relaxation mechanisms

The thermal relaxation Y consists of a number of steps: firstly, the hot electrons transfer their energy to the electron bath. This process is slightly faster than the electron-phonon relaxation[10,11]. The fast electron-electron relaxation results in a well-defined equilibrium electron bath temperature, hence Eq. 4.1. The electron-phonon interaction causes heat transfer towards the metal phonons with coefficient

$Y_R = \frac{C_V}{\tau_{eph}} \cdot d$ per unit area, with C_V the electron heat capacity, τ_{eph} the electron-phonon scattering time. We used Ref. [10,12] to calculate the τ_{eph} values for our Al and Nb layers respectively. The obtained values are listed in Table 4.1. The value of the electron-phonon heat transfer coefficient has to be compared to Kapitza conductance Y_K[13]. Since in our case $Y_K < Y_R$ at $T_{bath} = 4.2$ K the escape to the substrate is the slowest process.

4.5 Thermal healing length

With these numbers we can calculate a characteristic thermal healing length $\eta = (K \cdot d \,/\, Y_K)^{1/2}$[6]. Since the length is much larger than the thicknesses of the various layers and the width of the junction, the assumption of a constant temperature in the cylinder as sketched in Fig. 4.1 is justified.

TABLE 4.1. Material parameters for our layers needed in the calculation. The electrical conductivity σ is measured just above the transition temperature of Nb, and at 4.2 K for the Al layers. The heat conductivity K is calculated from the electrical conductivities. τ_{ee} and τ_{eph} are the electron-electron and electron-phonon relaxation times respectively, with the latter values the electron-phonon heat transfer coefficients Y_R are calculated. These have to be compared with the Kapitza conductances Y_K; the smaller value is used to determine the thermal healing length η.

	Nb	Al
σ $(\Omega\text{m})^{-1}$	$2.5 \cdot 10^7$ (10 K)	$2 \cdot 10^8$ (4.2 K)
K (W/mK)	0.4	18
τ_{ee} (ns)	1	0.4
τ_{eph} (ns)	2.5	0.8
Y_R (W/m^{2}K)	$50{\cdot}10^4$	$20{\cdot}10^4$
Y_K (W/m^{2}K)	$3{\cdot}10^4$	$6{\cdot}10^4$
η (μm)	3	5

The solution of Eq. 4.1 is:

$$T(r) \;=\; \frac{I \cdot V \;\eta}{\pi \; K \; d \; w \; \mathrm{K}_1(\frac{w}{2\eta}) \;\; (\cdot 2)} \;\cdot\; \mathrm{K}_0(\frac{r}{\eta}) \;+\; T_{bath} \qquad (4.2)$$

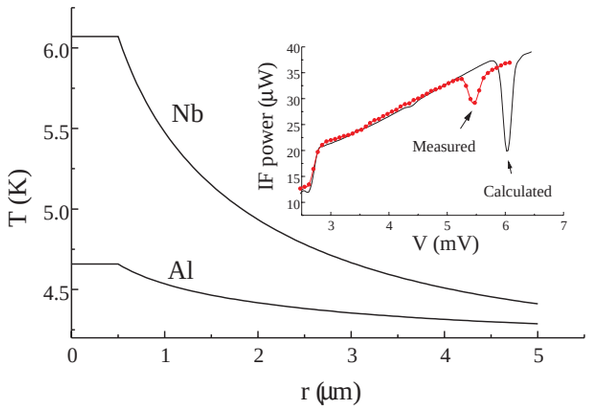

FIGURE 4.2. Calculated temperature profiles using Nb and Al leads. The insert shows (dots: experiment, full line: theory) the intermediate frequency (IF) power output in a heterodyne experiment, which is proportional to the differential resistance of the SIS junction. The apparent lower gap is indicative of intrinsic heating.

K_0 and K_1 are modified Bessel functions of the second kind. Eq. 4.2 is plotted in Fig. 4.2 and shows the temperature distribution in the leads for both the Nb and Al case for a 15 Ω junction at 5.5 mV. Fig. 4.3 shows the calculated temperature at $r = 0$ as a function of applied voltage. The plotted experimental values were obtained by measuring the first photon-assisted tunneling step above the gap. This step occurs at $V = (2\Delta + \hbar\omega)/e$. If at that voltage the temperature is higher the value of Δ is associated with the elevated temperature. This value is lower than the value of Δ at $V = 2\Delta/e$ and therefore the photon step occurs at a lower voltage. This voltage is measured for different frequencies to derive the gap value and the temperature using the BCS gap equation. The temperatures obtained from samples with different resistances are scaled to values corresponding to 15 Ω junctions. The difference between the use of Nb and Al leads is clear, from experiment as well as from the calculated values.

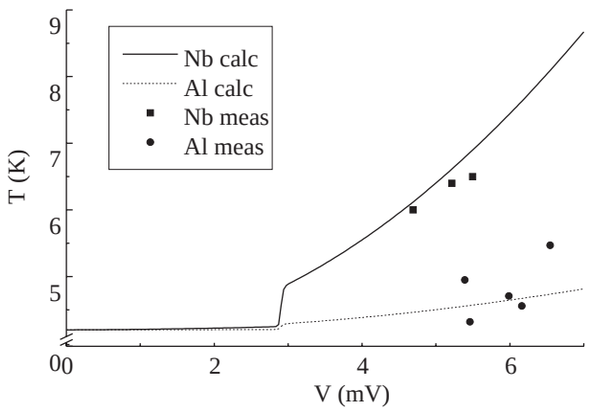

FIGURE 4.3. Temperature as function of applied voltage for a 15Ω junction. Calculated temperatures are presented as lines, measured temperatures are shown by dots.

4.6 Influence on mixer performance

To investigate the influence of the elevated temperature on the mixer performance, we calculated the subgap current increase at the operating voltage for heterodyne detection with the standard tunneling equation[14]. This approach is valid for high quality junctions in the temperature range of interest[15]. The DC power input results in an increased temperature of 0.05 K for a junction with Al leads and 0.39 K for Nb leads. The subgap current increase is 30% and 7% for Nb and Al leads respectively. To estimate the influence on the mixer noise temperature T_M we use the 3-port Tucker theory[16]. The increase in T_M at 460 GHz is 2% for the Nb case and 0.4% for a junction with Al striplines as compared to a junction without heating effects. Previously measured values[7] at the same frequency for an all-Nb junction suggested an increase of 4% and 1% for corresponding temperature increases. From these values we can conclude that the temperature increase during operation has little influence on the performance of the Nb SIS mixer.

4.7 Conclusions

A most promising result for the development of small area high current density THz mixers is that the area of the junction has little influence on the heating since the prefactor in Eq 2 is weakly dependent of the junction area w^2, because the $K_1(\frac{w}{2\eta})$ term in Eq. 2 nearly cancels the w term. Therefore the current density can be raised without severe additional heating effects if the total resistance is kept constant by decreasing the junction size. The only parameters effectively involved are the embedding configuration and the thermal conductivity of the embedding material. An example of the first is the use of junctions in series[4]; the thermal healing length is usually comparable to the spacing of the junctions, leading to a large effect on the temperature. An example of the effect of the thermal conductivity is the application of NbN as superconductor in SIS junctions and as low-loss stripline material. In using NbN junctions severe heating effects have been observed[17], which is partially due to the low thermal conductivity and partially due to the larger gap voltage of NbN, which requires a higher bias voltage. In both cases application of thick layers of clean highly conducting metals in an appropriate configuration is expected to improve the performance of the devices considerably.

References

[a)] Permanent address: Institute for Radio Engineering and Electronics, Russian Academy of Sciences, Mochoyova str. 11, Moskow 103907, Russia.

[1] H. van de Stadt, A. Baryshev, P. Dieleman, Th. de Graauw, T.M. Klapwijk, S. Kovtonyuk, G. de Lange, I. Lapitskaya, J. Mees, R.A. Panhuyzen, G. Prokopenko, and H. Schaeffer. *Proc. of the Sixth Int. Symp. on Space THz. Techn.*, California Institute of Technology, Pasadena, 1995, pp. 66-77.

[2] M. Bin, M.C. Gaidis, J. Zmuidzinas, T.G. Philips, and H.G. LeDuc, Appl. Phys. Lett. **68** 1714-1716 (1996).

[3] G. de Lange, C.E. Honingh, J.J. Kuipers, H.H.A. Schaeffer, R.A. Panhuyzen, T.M. Klapwijk, H. van de Stadt, and M.M.W.M. de Graauw, Appl. Phys. Lett. **64** 3039-3041 (1994).

[4] P. Febvre, W.R. McGrath, P. Batelaan, B. Bumble, H.G. LeDuc, S. George, and P. Feautrier, Int. Journ. Inf and MM waves, **15** (6) 943-966 (1994).

[5] M.M.T.M. Dierichs, R.A. Panhuyzen, C.E. Honingh, M.J. de Boer and T.M. Klapwijk, Appl. Phys. Lett. **15** 774-776 (1993).

[6] W.J. Skocpol, M.R. Beasley, and M. Tinkham, J. Appl. Phys. **45** (9) 4045 (1974).

[7] G. de Lange, Ph.D. thesis, University of Groningen, 1994.

[8] The value for the thermal conductivity was comparable to scaled down data from A. Boucheffa, M.X. François, and F. Koechlin, Cryogenics **34** 297 (1994).

[9] F. Pobell, *Matter and methods at low temperatures*, (Berlin, Springer-Verlag, 1992)

[10] P. Santhanam and D. Prober, Phys. Rev. B. **29** 3733-3736 (1984).

[11] D.E. Prober, Appl. Phys. Lett. **62** (17) 2119-2121 (1993), refers to the article of Santhanam and Prober to estimate the τ_{ee} in Nb for a nonequilibrium situation.

[12] E.M. Gershenzon, M.E Gershenzon, G.N. Gol'tsman, A.M. Lyul'kin, A.D. Semenov, and A.V. Sergeev, Sov. Phys. JETP **70**(3) 505-511 (1990).

[13] The Kapitza conductances are derived from the value measured for Sn on quartz in V.A. Holt, J. Appl. Phys. **37** (2) 798-802 (1965), and the squared ratio of the transmission coefficients for Sn, Nb, Al on SiO_2 table II in S.B. Kaplan, J. Low Temp. Phys. **37** 343 (1979).

[14] E.L. Wolf, *Principles of Electron Tunneling Spectroscopy*, (Oxford University Press, New York, 1985).

[15] R. Cristiano, L. Frunzio, R. Monaco, C. Nappi, and S. Pagano, Phys. Rev. **B 49** 429, (1994).

[16] J.R. Tucker, M.J. Feldman, Rev. Mod. Phys. **57**, 1055-1113, (1985).

[17] H. van de Stadt, J. Mees, Z. Barber, M. Blamire, P. Dieleman, and Th. de Graauw, Int. Journ. Inf. and MM waves **17** (1) 91-104 (1996).